Biosensors and Bioelectronics 25 (2010) 2038–2044

Contents lists available at ScienceDirect

Biosensors and Bioelectronics

journal homepage: www.elsevier.com/locate/bios

Nanostructured rough gold electrodes for the development of lactate oxidase-based biosensors

M. Gamero [a], F. Pariente [b,*], E. Lorenzo [b], C. Alonso [a]

[a] Department of Applied Physical Chemistry, Universidad Autónoma de Madrid, 28049 Madrid, Spain
[b] Department of Analytical Chemistry, Universidad Autónoma de Madrid, 28049 Madrid, Spain

ARTICLE INFO

Article history:
Received 23 October 2009
Received in revised form 25 January 2010
Accepted 26 January 2010
Available online 2 February 2010

Keywords:
Rough gold
Lactate oxidase biosensor
AFM
EIS

ABSTRACT

The design and characterization of a lactate biosensor using a nanostructured rough gold surface as a transducer is reported. The biosensor is developed by immobilization of lactate oxidase (LOx), on a rough gold electrode modified with a self-assembled monolayer of dithiobis-N-succinimidyl propionate (DTSP). This bifunctional reagent preserves the rough gold structure and allows further covalent immobilization of the enzyme through the terminal succinimidyl groups. The rough gold electrode is characterized using field emission scanning electron microscopy (FE-SEM) and atomic force microscopy (AFM). The preferential orientation and average crystallite size are obtained by X-ray diffraction (XRD). The resulting lactate oxidase monolayers are characterized by electrochemical impedance spectroscopy (EIS). This nanostructured transducer allows higher mediated electrocatalytic activity than polycrystalline ones. The biosensor response to increasing lactate concentrations, using hydroxymethylferrocene as a redox mediator in solution, is linear up to 1.2 mM with a sensitivity of 1.49 $\mu A\,mM^{-1}$.

1. Introduction

Lactate levels in blood or tissues are correlated to the presence of several diseases such as tissue hypoxia, cardiogenic or endotoxic shocks, respiratory failure and systemic disorders derived from neoplasic diseases, liver and renal failures or diabetes *mellitus*. Thus, the development of highly sensitive and reliable lactate monitoring methods are of great interest in clinical diagnostics (Burmeister et al., 2005; Patel et al., 2000), food technology (De Luca et al., 2005), beverage and fermentation industries (Zaydan and Dion. 2004) and clinical medicine (Volpe et al., 1995; Hart et al., 2004). Various procedures have been proposed for the direct measurement and monitoring of lactic acid levels in very different samples. The fundamentals, advantages and disadvantages of some of these methodologies have been summarised and compared in a recent review (Suman and Ashok Kumar, 2008). Among them, biosensors are one of the most widely investigated devices for two fundamental reasons: (1) the immobilization of an enzyme on the electrode surface may be done in an easy and reproducible way; and (2) the specificity of enzymes allows analytical measurements to be performed directly on the sample, regardless of their complexity, reducing the analysis time. Biosensors based on L-lactate oxidase (LOx) and L-lactate dehydrogenase (LDH) have been widely used for the determination of L-lactate (Palmisano et al., 1997; Parra et al., 2006; Jena and Raj, 2007). LOx-based biosensors are the most widely used configuration and allow the determination of hydrogen peroxide generated in the enzymatic reaction (Perdomo et al., 1999). The electrochemical determination of hydrogen peroxide involves high positive potentials and can be affected by the presence of interferents (Nikolaus and Strehlitz, 2008). On the other hand, the sensitivity of the biosensor depends on the molecular oxygen concentration (Palmisano et al., 2001; Moser et al., 2002). One strategy used to avoid these problems is to replace the natural electron acceptor (O_2) with an artificial mediator, such as hydroxymethylferrocene (Boujtita et al., 1996; Parra et al., 2006).

Recent reports show that the use of nanostructured electrode surfaces can improve the performance of electrochemical sensors and biosensors (Lupu et al., 2007).

Nanostructured electrode surfaces can be obtained in a variety of ways, such as the modification of surfaces with nanostructured materials or nanopatterning of the electrode surface itself. In this sense, gold electrodes can quickly and easily be nanostructured by electroreducing the thick accumulated oxide layers by applying relatively fast periodic potentials in acid solutions (Vazquez et al., 1989). This nanopatterning process gives rise to rough gold electrodes with a larger active area that can be used in the design of significantly improved lactate biosensors.

One key factor in the development of a reliable biosensor is the immobilization process, which affects most of the analytical properties of the device (Sung and Bae, 2006). Several methods for the immobilization of LOx on different types of electrodes have been reported. Most of them involve covalent immobilization (Nikolaus

* Corresponding author. Tel.: +34 91 497 8625; fax: +34 91 497 4931.
E-mail address: felix.pariente@uam.es (F. Pariente).

0956-5663/$ – see front matter © 2010 Elsevier B.V. All rights reserved.
doi:10.1016/j.bios.2010.01.032

and Strehlitz, 2008). In our experience, covalent immobilization onto gold electrodes gives rise to more reproducible results (Parra et al., 2006). In the present work, dithiobis-N-succinimidyl propionate (DTSP) is used to modify the nanostructured gold electrode surface. This bifunctional reagent forms self-assembled monolayers preserving the rough gold structure and allowing further covalent immobilization of the enzyme through the terminal succinimidyl groups.

Microscopic, impedimetric and voltammetric techniques have been used to characterize the morphology and physical properties of the resulting biosensor. Its electrocatalytic response has been studied and compared to that obtained under the same conditions with a polycrystalline gold electrode.

2. Materials and methods

2.1. Reagents and solutions

Lactate oxidase (EC 232-841-6 from *Pediococcus* species) lyophilized powder containing 41 units/mg solid was obtained from the Sigma Chemical Co. (St. Louis, MO). Stock solution was prepared by dissolving 1.3 mg of the LOx lyophilised powder in 250 μL of 0.1 M phosphate buffer (PBS) pH = 7.0, aliquoted (10 μL) and stored at −30 °C. Under these conditions, the enzymatic activities remain stable for several weeks. A stock solution of L-(+) lactic acid lithium salt 97% (from Sigma Chemical Co) was prepared by dissolving 9.9 mg of the product in 1 ml of 0.1 M PBS (pH = 7.0) containing 1 mM hydroxymethylferrocene. 3,3′-dithiodipropionic acid di(N-succinimidyl ester) (DTSP), hydroxymethylferrocene and dimethyl-sulfoxide (DMSO) were obtained from Aldrich Chemical Co. (Milwaukee, WI) and used as received. Other chemicals used in this work, such as sulphuric acid and sodium phosphate, were reagent grade quality and used as received without additional purification steps. Sodium phosphate (Merck) was employed for the preparation of buffer solutions (0.1 M, pH 7.0). All the solutions were prepared with ultra pure water by means of a Millipore Milli-Q system (18.2 MΩ^{-1}).

2.2. Electrochemical cell

An electrochemical cell with a three-electrode set-up was used. The working electrode was a gold wire (99.99% purity) of 1 mm in diameter connected to a metallic clip to make electrical contact and masked with teflon tape to leave a free geometric area of 0.06 cm^2. Gold electrodes with roughness $R = 1.5$ and $R = 66$ were prepared. The rough gold electrode was maintained in water at temperature of 4 °C in order to avoid the relaxation of the structure (Alonso et Salvarezza, 1990), since relaxation depends on the temperature (Alonso et al., 1990). This structure is fixed when the SAM monolayer is formed. A large area platinum electrode was used as counterelectrode. All the potentials are quoted with respect to a mercury/mercurous sulphate reference electrode (MSE). The electrochemical area of the working electrode was measured in 0.5 M H_2SO_4 by integration of the charge required for reduction of an oxidised gold surface produced in a previous anodic scan up to +1.1 V vs. MSE. A conversion factor of 400 μC.cm^{-2} was used (Brumer and Makrides, 1964). The experiments were performed in solutions thermostated at 25 °C ± 0.5 °C.

2.3. Preparation of electrodispersed Au electrodes

The procedure was carried out in two consecutive stages. Firstly, the hydrous metal oxide layer (HMOL) was accumulated on a polycrystalline Au electrode immersed in 0.5 M sulphuric acid by applying a repetitive square wave perturbing potential (RSWPP) at 4 kHz between −0.045 V and 2.456 V (MSE) for a time of 2 min to form a thick hydrous gold oxide layer. In this case τ_u and τ_l, the positive and negative half-cycle times, were 0.15 ms and 0.10 ms respectively. In the following stage, the HMOL was voltammetrically electroreduced at 0.02 Vs^{-1} as previously described (Vazquez et al., 1989). At this potential sweep rate the Au overlayer growth rate is close to 10^{-5} cm.s^{-1}, resulting in the maximum development of roughness (Salvarezza et al., 1990).

The electrochemical evaluation of the Au overlayer roughness (R) for the working electrode was made from the voltammetric charge ratio between the O-adatom electrodesorption charge determined for the rough Au electrode and that of the starting polycrystalline Au electrode, measuring both charges by voltammetry under exactly the same potential limits and potential sweep conditions (Fig. 1S). (Gomez et al., 1988).

2.4. SEM, XRD and AFM characterization

The equipment used for the characterization of rough Au samples was a Philips XL30 Scanning Electron Microscope equipped with a Field Emission Gun (FEG) and coupled with an Energy Dispersive X-ray analyzer. (EDX DE4i). The samples were examined at 15 keV acceleration voltages.

The phases present in the coating were determined by X-ray diffractometry (see supporting information for more details).

For the atomic force microscopy (AFM) studies, a Nanoscope IIIa Multimode from Veeco equipment was used. The measurements were carried out using Antimony (n) doped Si cantilevers (Model TESP-SS; 2 nm < r < 5 nm; nominal spring constant of 42 N/m) from Veeco. The images were flattened, off-line, using zero-or-first-order polynomial fits to account for Z offsets and sample tilt. Tapping-mode AFM was used for morphological imaging of the polycrystalline and rough gold samples.

2.5. Electrochemical impedance spectroscopy (EIS) measurements

EIS experiments were performed with an Autolab PGSTAT 30 potentiostat from Eco-Chemie. The solution was 0.1 M PBS (pH = 7), 0.1 M KCl containing 10 mM $K_3Fe(CN)_6$ + 10 mM $K_4Fe(CN)_6$. A sinusoidal potential modulation of ±10 mV amplitude in 10^5 Hz–10^{-3} Hz frequency range, spaced logarithmically (120 per 8 decades), was superimposed on the formal potential of the redox couple $[Fe(CN)_6]^{3-/4-}$ (−0.21 V vs.MSE). To obtain the capacitance from experimental data, a frequency f_i to obtain a maximum value of phase angle (θ) was selected. The capacitance was calculated as $C = 1/(2\,\pi f i Z i)$, where Zi is the imaginary part of the impedance at frequency, f_i.

EIS results were analysed by fitting the experimental impedance data to electrical equivalent circuit models. The electrical equivalent circuit parameters were calculated by fitting the impedance function to the measured spectra with a non-linear least-squares (NLLS) program using Z-plot/Z-view for all the frequencies measured. The criteria used to estimate the fitting quality were evaluated firstly with the low chi-square value and secondly with the low estimative errors (%) for all the components.

2.6. Procedures

DTSP-functionalised gold electrodes and biosensor preparation.

Gold electrodes were immersed for 3 h at room temperature in a fresh solution of 4.0 mM DTSP in DMSO (Au-DTSP). The corresponding monolayer containing the active succinimidyl esters was subsequently rinsed in DMSO and PBS.

10 μL of LOx stock solution was placed on the DTSP-modified polycrystalline (Au) or rough (Au_R) gold electrode. After air-drying, the biosensor (Au-DTSP-LOx) was washed with 0.1 M PBS pH = 7 to remove any weakly bound enzyme.

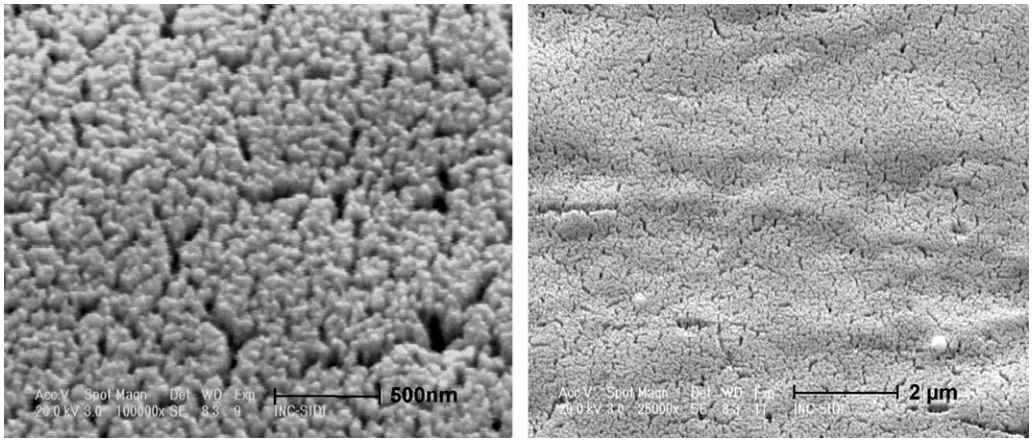

Fig. 1. SEM images of rough gold electrode at different magnifications: 500 nm and 2 μm.

3. Results and discussion

3.1. Characterization of the nanostructured transducer surface

The surface morphology of the rough gold deposits was observed by field emission scanning electron microscopy (FE-SEM) and by AFM, obtaining the preferential orientation and average crystallite size by X-ray diffraction (XRD).

Fig. 1 shows the micrographs of the rough gold ($R = 66$) obtained by FE-SEM at two different magnifications. SEM images show the brain-like appearance previously reported (Vazquez et al., 1989) as characteristic of gold overlayers resulting from the electroreduction process, revealing the presence of small grains and channels of about 150 nm in width. In fact, the most characteristic features are the voids and not the grains. This brain-like appearance remains similar even though the roughness changes. Considering that the roughness is due to the area of 3D electrodeposits formed by a rectangular array of columns of average height h and average radius r terminated with a hemispherical dome of the same radius, of C_{4v} symmetry, it is possible to estimate these parameters from the electrochemical data (Vazquez et al., 1989). The electroreduction of the gold oxide layer to form the gold overlayer can be represented by the following reaction:

$$Au_2O_3 + 6H^+ + 6e^- \rightarrow 2Au + 3H_2O$$

The thickness of the metal overlayer can be obtained from the equation

$$h = Mq/ZF\rho \quad (1)$$

where M and ρ are the gold atomic weight (196.96 g.mol^{-1}) and the density of the gold electrodeposit (19.32 g.cc^{-1}), respectively. Taking $Z = 3e^-$, h becomes 3.8 10^{-5} cm for an electroreduction charge of $q = 1.07$ C.cm^{-2}. In a similar way, the average radii r of 6 nm may be obtained from the following equation:

$$R = (\pi/3)(h/r) \quad (2)$$

The AFM image (Fig. 2) (1 μm × 1 μm) shows the difference between the surface structure of an untreated polycrystalline gold whose roughness is $R = 1.5$ and a rough gold surface ($R = 66$). AFM reveals the development of a rounded cap columnar-type structure. It should be noticed that some large grains (80–100 nm) are formed by nanometric subunits (20–40 nm). The image shows a channel of about 150 nm in width. Along the channel, it is possible to see the grain structure indicating columnar growth. Topographic analysis (Fig. 2S) for both substrates reveals that the average height is close to 280 nm for rough gold and 30 nm for the polycrystalline gold substrate. Moreover, it can be seen that the height distribution is more uniform when there is a columnar structure. However, the column height values obtained from AFM measurements are lower than those obtained from the theoretical model and the radius is higher. This may be due to the AFM limitation and the ageing process, characterized by a coalescence of grains with time due to surface diffusion of adatoms from sites of higher chemical potential to sites of lower potential in order to minimise the total free surface energy of the system (Alonso et al., 1990).

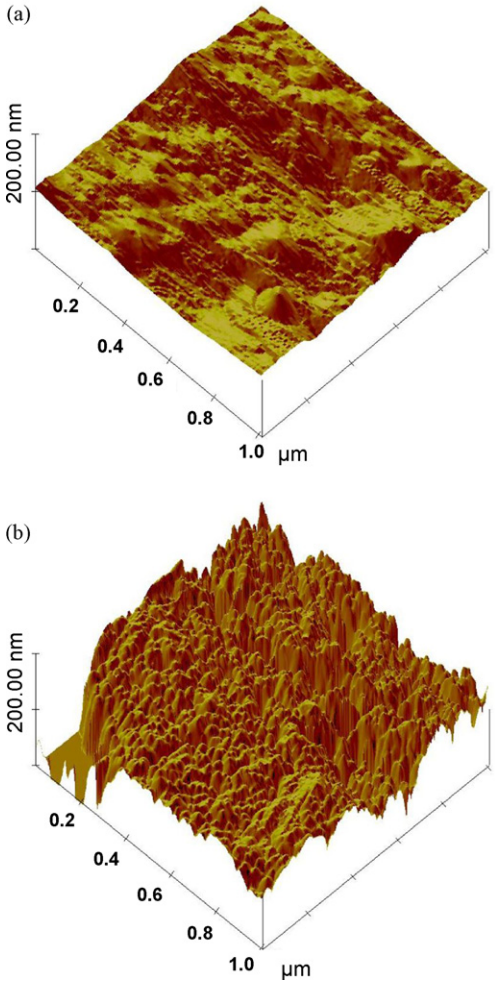

Fig. 2. 1 μm × 1 μm tapping-mode AFM images of (a) polycrystalline gold electrode $R = 1.5$ (b) rough gold electrode $R = 66$.

Gold crystallises in the cubic system with $\alpha = \beta = \gamma = 90^\circ$ and $a = b = c = 4.0786$, the main crystallographic planes being (111), (100) and (110). Figure 3Sa shows the diffractogram obtained for polycrystalline gold with the XRD peak of the greatest intensity corresponding to orientation (111). A similar diffractogram is obtained for rough gold (Fig. 3Sb), with two exceptions: the measured intensity ratio between preferential orientations (111) and (200) has a very high value (8.8) compared to that obtained for untreated gold (2.5); and the relative intensity of the diffraction peak corresponding to orientation (311) is very small. This preferential orientation can be observed in Figure 1Sb, where a change in the voltammetric profile related to the electroadsorption of O atoms on Au can be seen. In general, the intensity of the peaks for polycrystalline gold is smaller, with a higher signal/noise ratio than that obtained for rough gold due to the fact that the sample is less crystalline. Therefore, the rough gold electrode exhibits a more crystalline structure than the polycrystalline electrode, as well as a preferential orientation (111). On the other hand, the coalescence of the rough structure also involves a preferential orientation. In this case, the X-ray diffraction peak of the greatest intensity corresponds to orientation (311) (Fig. 3Sc).

Calculation of the average grain size for the rough gold was performed from the X-ray diffraction peak of the greatest intensity, corresponding to orientation (111). Applying Scherrer's equation (Cullity, 1978) an average value of 589 Å is obtained. The average crystallite size for polycrystalline gold is higher: 768 Å.

3.2. Electrochemical impedance spectroscopy

EIS is an effective method for probing the interfacial properties of modified electrodes and a noninvasive way of monitoring each step in the construction of biosensors, in contrast to voltammetric methods.

The Bode diagrams of the Au_R, Au_R-DTSP and Au_R-DTSP-LOx are shown in Fig. 3(a,b). The impedance modulus Bode diagrams present a plateau at high frequencies. The impedance value in this region, with $\varphi = 0$, gives the electrolyte resistance (R_e) in each case. For Au_R and Au_R-DTSP, at decreasing frequencies (10^2 Hz–10^{-2} Hz), a single slope is observed, with a phase angle close to -45° associated to a diffusion process. However, for Au_R-DTSP-LOx, two slopes and two phase-angles associated to a kinetic process (high frequencies) and a diffusion process (low frequencies) are observed. In the lower frequency range (10^{-2} Hz–10^{-3} Hz), the phase angle is close to 0°, corresponding to a plateau in the impedance modulus versus frequency plot. From this region it is possible to obtain the total resistance of the circuit (W_R,R_{TC}, R_e).

The Nyquist diagrams show two frequency regions (Fig. 3c). At high frequencies (10^4 Hz), the semicircle parts correspond to the charge transfer resistance limiting process associated to either Au_R-DTSP or AuR-DTSP-LOx/electrolyte (R_{TC}). The intercept with the real axis, at high frequencies (10^4 Hz), correspond to electrolyte resistance (Re). At low frequencies, the linear part is due to the diffusion process control with the particularity that at very low frequencies, Z' approaches the Warburg resistance (W_R) and Z" goes to zero. This behaviour is characteristic of diffusion through a finite length diffusion layer.

The impedance diagrams have been fitted considering the electrical equivalent circuits of Fig. 3. The following electronic elements have been chosen in the circuit: R_e, the electrolyte resistance measured between the working and reference electrodes; R_{TC}, the charge transfer resistance, and; CPE1, a constant phase element simulating a non-ideal behaviour of the capacitor. R_{TC} and CPE1 correspond to the outer interface (depending on Au_R modified or unmodified). W_R is a finite length Warburg element and represents the diffusion through a porous structure of rough gold. In this circuit, a distributed element is used instead of a capacitor. Its impedance is $Z = 1/[T(jw)^n]$ and is generally used when there is a distribution of relaxation times as a result of inhomogeneities present on the surface.

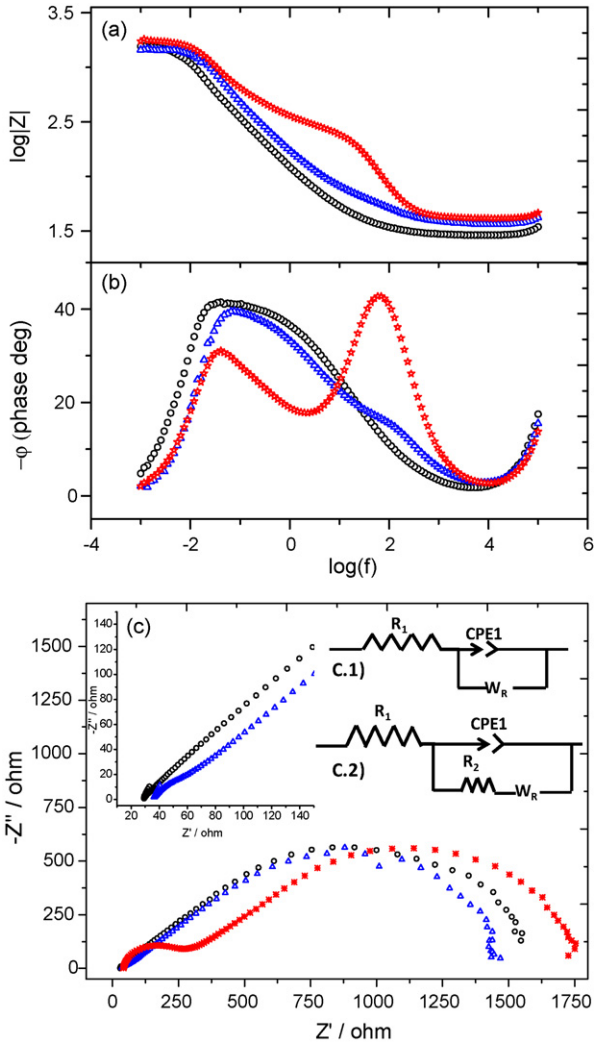

Fig. 3. Impedance modulus and phase angle diagrams vs frequency of the Bode plots (a, b) and Nyquist diagrams (c) for Au_R (o) Au_R-DTSP (Δ) Au_R-DTSP-LOx (*) in 0.1 M KCl/0.1 M phosphate buffer solution (pH = 7) containing 10 mM $[Fe(CN)_6]^{3-}$ + 10 mM $[Fe(CN)_6]^{4-}$. Inset: Magnification of Nyquist plots for Au_R, Au_R-DTSP; fitting circuits C1 for Au_R and C2 for AuR-DTSP, Au_R-DTSP-LOx.

The results obtained from the fitting for Au_R, Au_R-DTSP and Au_R-DTSP-LOx are given in Table 1. For comparative purposes, the capacitance (C_1) calculated from experimental data, has been also included, as well as the other experimental parameters.

Considering the results obtained from the impedance spectra measured for Au_R (Table 1), it can be seen in the Nyquist diagrams (Fig. 3c, inset), that in the frequency interval imposed the semicircle corresponding to a charge transfer process is not observed. Instead of this, a straight line with a slope of 0.92 and an angle of 42.6°, which clearly corresponds to a diffusion process is obtained. However, for Au_R–DTSP a semicircle appears, showing a charge transfer resistance (R_{TC}) of 3.15 $\Omega.cm^2$ which increases to 18.90 $\Omega.cm^2$ for Au_R–DTSP- LOx (Table 1).

The impedance increase demonstrates that the adsorbed DTSP molecules and the bound enzyme prevent electron transfer between the ferro/ferricyanide molecules and the electrode surface. Since the amplitude of the sinusoidal perturbation is small ($\pm$ 10 mV) it is possible to use the linearised i-η characteristic and

Table 1
Experimental and fitting results from EIS experiments for rough gold electrode.

	Au_R	Au_R-DTSP	Au_R-DTSP-LOx
Experimental results			
Re (Ω)	*29.10*	*35.90*	*41.07*
R_{TC} (Ω·cm^2)	*0*	*3.15*	*18.90*
K^0 (ms^{-1})	–	*8.58 10^{-5}*	*1.43 10^{-5}*
C_1 (F·cm^{-2})	*8.81 10^{-4}*	*7.84 10^{-4}*	*4.18 10^{-4}*
T_{TC} (s)		*6.81 10^{-3}*	*7.91 10^{-3}*
W_R (Ω·cm^2)	*159.26*	*67.2*	*109.2*
T_ω (s)	*13.37*	*7.19*	*8.40*
σ (Ω·cm^2·s$^{-1/2}$)	*17.25*	*10.71*	*15.44*
k (s$^{1/2}$)	*8.24*	*6.04*	*6.53*
δ (μm)	*2.15*	*1.15*	*1.35*
b	*−0.92(42.6°)*	*−0.92(42.6°)*	*−0.82(40°)*
Fitting results			
Re (Ω)	*28.67*	*35.9*	*41.54*
R_{TC} (Ω·cm^2)	*0*	*1.15*	*15.74*
CPE1(S·s^{n}cm^{-2})	*4.69 10^{-3}*	*4.87 10^{-3}*	*5.13 10^{-4}*
n	*0.74*	*0.75*	*0.93*
W_R (Ω·cm^2)	*163.58*	*69.95*	*113.25*
W_T	*38.36*	*16.55*	*21.95*
W_P	*0.46*	*0.48*	*0.46*
X^2	*2.4 10^{-4}*	*9.3 10^{-4}*	*2.1 10^{-4}*

hence to obtain the response of heterogeneous charge-transfer kinetics:

$$R_{TC} = RT/nFi^0 \quad (3)$$

Where the exchange current i^0 is given by Equation (4)

$$i^0 = nFAk^0C \quad (4)$$

where k^0 is the electron transfer rate constant between the ferro/ferricyanide probe molecule redox couple and the electrode; C is the concentration of the redox couple in the bulk solution; n is the number of electrons involved in the electrode reaction; A is the electrode area; R the universal constant of ideal gases; T is the temperature and F is the Faraday constant. The k^0 value for the redox probe on the Au_R electrode modified with DTSP was 8.58 10^{-5} m.s^{-1}. The enzyme adsorption on the Au_R-DTSP electrode resulted in a charge transfer rate constant six times lower (Table 1). Subsequently, the pseudocapacitance decreases from 3.26 10^{-3} F.cm^{-2} for Au_R-DTSP, to 4.66 10^{-4} F.cm^{-2} for the Au_R-DTSP-LOx. The same trend is observed in the capacitance values obtained from the equivalent electric circuit. It is worth noting that the value of n, associated to CPE1, increases with the presence of the enzyme, indicating an increase in the capacitative character of the interface enzyme/solution. These capacitance values are 40 times greater than that of the polycrystalline gold electrode (1,1510^{-5} F.cm^{-2}).

The time constant of the corresponding charge transfer process can be calculated from the maximum frequency value, ω_{max}, in which the semicircle draws a maximum in the imaginary axis, and is done using the equation (Bastidas et al., 1986)

$$\tau_{TC} = 1/\omega_{max} = R_{TC}\,C_1 \quad (5)$$

The time constant value decreases from 1.02 10^{-2} s for Au_R-DTSP to 8.80 10^{-3} s for Au_R-DTSP-LOx.

For high frequencies, the Nyquist diagram represents diffusion impedance (Warburg resistance, W_R) through a finite length diffusion layer, i.e. ionic diffusion through a porous structure. The values obtained for W_R are about 100 Ω.cm^2. Furthermore, in this frequency range the slope value (Z" vs. Z'), which is close to unity, together with the phase angle value (close to 45°) and the W_P value (Table 1), indicate that the process is controlled by ionic diffusion. These facts are more evident in the impedance modulus and shift-phase angle versus frequency Bode diagrams (Fig. 3b) for the Au_R-DTSP-LOx. The system clearly shows two different slopes (two different time constants τ_{TC}, τ_w), one at high frequencies corresponding to a kinetic control process and other at low frequencies related to a diffusion control process with θ_{Max} −42.74 (59.30 Hz) and −31.07 (0.04 Hz), respectively.

The time constant for the diffusion process can be obtained from:

$$\tau_w = 1/\omega^w_{max} = K^2/5.08 \quad (6)$$

where $\omega^w{}_{max}$ is the frequency value at which the second semicircle draws a maximum on the imaginary axis. From $\omega^w{}_{max}$, it is also possible to calculate the K constant defined by Dawson and John (1980) $K = \delta(2/D)^{1/2}$, where D is the diffusion coefficient of the ionic species and δ is the thickness of diffusion layer. For the diffusion controlled system the K constant is related with the real part of the Warburg impedance (W_R) by the Warburg coefficient σ, being $W_R = \sigma K$. This parameter is used as a diagnostic criterion. In this case, the Nyquist diagram is typical of a system with $R_{TC} \ll \sigma K$. The values obtained for these parameters are shown in Table 1.

For comparative purposes, a similar study was performed on a polycrystalline gold electrode modified either with DTSP (Au-DTSP) or DTSP and lactate oxidase (Au-DTSP-LOx) (Fig. 4S). The experimental values and the values obtained from the equivalent electric circuit are shown in Table 1S. The most outstanding fact is that for the Au-DTSP-LOx the charge transfer resistance (R_{TC}) is about four times higher than that for the Au_R-DTSP-LOx biosensor and the electron transfer rate constant (k^0) is one order of magnitude lower. It is noticeable that for high frequencies the Nyquist diagram represents diffusion impedance (W_R) through a porous structure. This can be due to that $[Fe(CN)_6]^{3-/4-}$ ions diffuse through the pores left by the enzyme.

3.3. Biosensor response

The immobilised LOx oxidises L-lactate to pyruvate in the presence of hydroxylmethylferrocene, acting as an acceptor of the electrons generated in the enzymatic reaction and becoming transformed to their reduced form. This mediator in turn diffuses to the electrode, where it is reoxidised back to its oxidised form. The electrode acts as a secondary acceptor of electrons, regenerating the redox mediator used in the enzymatic reaction according to the following reaction pathway:

$$\text{L-lactate} + (\text{LOx})_{ox} \rightarrow \text{pyruvate} + (\text{LOx})_{red} \quad (1)$$

$$(\text{LOx})_{red} + (\text{HMF})_{ox} \rightarrow (\text{LOx})_{ox} + (\text{HMF})_{red} \quad (2)$$

$$(\text{HMF})_{red} \rightarrow (\text{HMF})_{ox} + e^- \quad (3)$$

This sequence of redox events represents a catalytic process. Thus, the magnitude of the catalytic current can be employed as the analytical signal in the determination of the lactate concentration. Fig. 4 depicts the cyclic voltammetric response for both Au-DTSP-LOx and Au_R-DTSP-LOx electrodes in 0.1 M PBS (pH = 7) containing 1.0 mM hydroxylmethylferrocene (HMF), in the absence (curve a) and in the presence (curve b) of substrate. In the absence of substrate, as would be anticipated, a redox response ascribed to the ferrocene/ferrocinium process is obtained (E_{pa}–E_{pc} = 80 mV). Upon addition of lactate, the cyclic voltammogram exhibits an enhancement of the anodic peak current concomitant with a decrease of the cathodic peak current. This behaviour is consistent with a strong electrocatalytic effect and is more evident for Au_R-DTSP-LOx (Fig. 4B).

To confirm the role of the LOx in the catalytic response to substrate, modified DTSP polycrystalline or rough gold electrodes without LOx, were immersed in 0.1 M PBS (pH = 7.0) containing 1.0 mM HMF. The results obtained in both systems confirm that the addition of lactate did not cause any catalytic effect associated with the ferrocene/ferrocinium process.

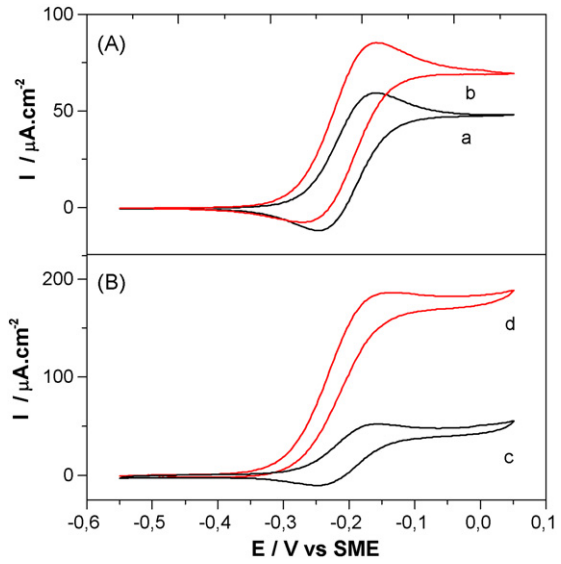

Fig. 4. Cyclic voltammograms for lactate oxidase immobilized onto a DTSP-modified gold electrode: polycrystalline (Au-DTSP-LOx) (A) and rough (Au_R-DTSP-LOx) (B) in absence of substrate (curves a and c) and in presence of 14 mM of L-lactate (curves b and d). (ν = 10 mV.s^{-1}).

Figure 5S depicts calibration curves obtained by plotting the catalytic current, obtained from CV measurements, at the same experimental conditions described above, versus increasing L-lactate concentrations ranging from 0.0 to 10 mM and 0.0 to 14 mM for (A) Au-DTSP-LOx and (B) Au_R-DTSP-LOx electrodes, respectively. Each data point represents the mean of three replicate measurements, and the scatter of individual measurements from this value is indicated. In both cases Michaelis-Menten behaviour is observed, which suggests that the electrochemical response is under enzymatic control. The experimental data were fitted to a Michaelis-Menten equation by means non-linear regression to calculate the K'_M value. This value indicates the grade of affinity of the immobilised enzyme to the substrate and provides the substrate concentration range over which the electrode response is linear. K'_M values of 0.27 and 0.93 were calculated for LOx bound to Au-DTSP-LOx and Au_R-DTSP-LOx, respectively. The increase in the magnitude of K'_M extends the upper limit of the linear response (Table 2).

The analytical properties (Table 2) of both Au-DTSP-LOx and Au_R-DTSP-LOx biosensors were obtained from the linear part of the calibration curve. Au_R-DTSP-LOx electrodes show a wider linear response than that obtained for Au-DTSP-LOx (inset of Figure 5SB), since the former allows a higher enzyme loading. The sensitivity values, calculated from the slopes of the plots, were 0.99 μA mM^{-1} and 1.49 μA mM^{-1} for Au-DTSP-LOx and Au_R-DTSP-LOx, respectively. Although the rough surfaces provide higher sensitivity, the detection and determination limits (21,5 μM and 71,8 μM, respectively) do not improve when compare to the polycrystalline gold (14 μM and 48 μM, respectively). The relative standard deviation for three successive measurements was 3% and the reproducibility, using five different biosensors was 10%. These values were similar to those found for Au-DTSP-LOx (2% and 8%, respectively).

Concerning the stability of biosensor, it was found that the response decrease around 15% of its initial value after one assay and then it remains constant after three days. These results show that there are not significant differences in stability between Au-DTSP-LOx and Au_R-DTSP-LOx biosensors. Between measurements, biosensors were stored in a PBS at 4 °C.

Regarding potential interferents, the Au_R-DTSP-LOx biosensor response in the presence of 0.1 mM of several substances, such as tartaric acid, citric acid, ascorbic acid, glucose and fructose was obtained. It was very similar to that observed for Au-DTSP-LOx, where these interferents studied did not change the biosensor response except in the case of ascorbic acid.

Table 2

	Au-DTSP-LOx	Au_R-DTSP-LOx
Linear response (mM)	*Up to 0.2*	*Up to 1.2*
K_M (mM)	*0.270 ± 0.007*	*0.93 ± 0.06*
I_{MAX} (μA cm^{-2})	*85.2*	*186.2*
Sensitivity (μA mM^{-1})	*0.99*	*1.49*
Detection limit (μM)	*14*	*21.5*
Determination limit (μM)	*48*	*71.8*
Reproducibility (R.S.D.)	*2.9%*	*3.9%*
Repeatability (R.S.D.)	*0.3%*	*0.5%*

[1]The detection limit was calculated from the ratio of 3 times the standard deviation of background and the sensitivity.
[2]The determination limit was calculated from 10 times the standard deviation of background current by the sensitivity.
[3]The reproducibility was evaluated comparing the signals obtained using five different biosensors prepared from the same LOx batch for a lactate concentration of 0.5 mM.
[4]The repeatability was evaluated from three measurements of a lactate concentration of 0.6 mM with the same biosensor.

4. Conclusions

A comprehensive study of a rough gold electrode as a general transducer in the development of bioanalytical platforms for biosensor applications has been described. In particular, emphasis has been placed on electrochemical biosensors based on LOx, which was immobilised by covalent binding to these new electrode surfaces modified with DTSP. Different surface characterization techniques (SEM, AFM, XRD) have been employed to characterize this nanostructured surface, which has the advantage of presenting a large specific area, enabling high enzyme loading and decreasing the charge transfer resistance, as can be concluded from EIS experiments. As a consequence, the resulting biosensor exhibits a wider linear range concentration and higher sensitivity compared to a polycrystalline gold electrode. Taking into account the good performance of the resulting biosensor, this nanostructured gold electrode surface is a promising transducer for the development of bioanalytical platforms.

Conflicts of interest

The authors have not declared any conflict of interest.

Acknowledgements

This work has been supported by the Ministerio de Ciencia y Tecnología of Spain through CTQ2008-05775/BQU Grant.

Appendix A. Supplementary data

Supplementary data associated with this article can be found, in the online version, at doi:10.1016/j.bios.2010.01.032.

References

Alonso, C., Salvarezza, R.C., Vara, J.M., Arvia, A.J., Vazquez, L., Bartolome, A., Baro, A.M., 1990a. J. Electrochem. Soc. 137 (7), 2161–2166.
Alonso, C., Salvarezza, R.C., Vara, J.M., Arvia, A.J., 1990b. Electrochimica Acta 35 (9), 1331–1336.
Bastidas, J.M., Feliu, S., Morcillo, M., 1986. Rev. Metal. 22 (2), 120–129.
Boujtita, M., Chapleaua, M., El Murr, N., 1996. Electroanalysis 8, 485–488.
Brumer, S.B., Makrides, A.C., 1964. J. Electrochem. Soc. 111, 1122.
Burmeister, J.J., Palmer, M., Gerhardt, G.A., 2005. Biosens. Bioelectron. 20, 1772–1779.

Cullity, B.D., 1978. Elements of X-ray Diffraction, 2nd ed. Addison-Wesley Publishing Company, Ch 9, p. 284.
Dawson, J.L., John, D.G., 1980. J. Electroanal. Chem. 110, 37–47.
De Luca, S., Florescu, M., Ghica, M.E., Lupu, A., Palleschi, G., Brett, C.M.A., Compagnone, D., 2005. Talanta 68, 171–178.
Gomez, J., Vazquez, L., Baro, A.M., Alonso, C., Gonzalez, E., Gonzalez-Velasco, J., Arvia, A.J., 1988. J. Electroanal. Chem. 240, 77–88.
Hart, J.P., Crew, A., Crouch, E., Honeychurch, K.C., Pemberton, R.M., 2004. Anal. Lett. 37, 789–793.
Jena, B.K., Raj, C.R., 2007. Electroanalysis 7 (8), 816–822.
Lupu, A., Valsesia, A., Bretagnol, F., Colpo, P., Rossi, F., 2007. Sens. Actuators B 127, 606–612.
Moser, I., Jobst, G., Urban, G.A., 2002. Biosens. Bioelectron. 17, 297–302.
Nikolaus, N., Strehlitz, B., 2008. Microchim. Acta 160, 15–55.
Palmisano, F., De Benedetto, G.E., Zambonin, C.G., 1997. Analyst 122, 365–369.
Palmisano, F., Quinto, M., Rizzi, R., Zambonin, P.G., 2001. Analyst 126, 866–870.
Parra, A., Casero, E., Vazquez, L., Pariente, F., Lorenzo, E., 2006. Anal. Chim. Acta 555, 308–315.
Patel, N.G., Erlenkotter, A., Cammann, K., Chemnitius, G.C., 2000. Sens. Actuators B: Chem. 67 (1,2), 134–141.
Perdomo, J., Sundermeier, C., Hinkers, H., Martinez, M.O., Seifert, W., Knoll, M., 1999. Biosens. Bioelectron. 14, 27–32.
Salvarezza, R.C., Alonso, C., Vara, J.M., Albano, E., Martin, H.O., Arvia, A.J., 1990. Phys. Rev. B. 41 (12), 502–512.
Suman, Ashok Kumar, 2008. Sens. Transducers J. 96 (9), 18–31.
Sung, W.J., Bae, Y.H., 2006. Sens. Actuators 114, 164–169.
Vazquez, L., Bartolome, A., Baro, A.M., Alonso, C., Salvarezza, R.C., Arvia, A.J., 1989. Surf. Sci. 215, 171–189.
Volpe, G., Moscone, D., Compagnone, D., Palleschi, G., 1995. Sens. Actuators B 24, 138–141.
Zaydan, R., MDion, M., Boujtita, M., 2004. J. Agric. Food Chem. 52 (1), 8–14.